Oxygen isotopic composition of a compound Ca-Al-rich inclusion from Allende meteorite: implications for origin of palisade bodies and O-isotopic environment in the CAI forming region

Guk Lac KIM*, ***, Hisayoshi YURIMOTO** and Shigeho SUENO*

* Institute of Geosciences, University of Tsukuba, Tsukuba,
Ibaraki 305, Japan
**Department of Earth and Planetary Sciences, Tokyo Institute of Technology, Meguro,
Tokyo152-8551, Japan
*** Present address: Department of Mineral Sciences, National Museum of Natural History,
Smithsonian Institution, Washington, DC 20560-0119 USA

A calcium-aluminum-rich inclusion (CAI) containing big palisade bodies was found within the Allende meteorite. The bulk composition and mineral assemblages show that the CAI belongs to coarse-grained Type B. Oxygen isotopic distributions in palisade bodies in the CAI are similar to those observed in typical Type B CAIs, whereas all minerals including melilite in the host parts are enriched in ^{16}O. The oxygen isotopic distribution in the CAI indicates that exchange of oxygen isotopes in the palisade bodies occurred before the trapping of palisades into the host. The palisade bodies were formed separately as small CAIs in the solar nebula and then accumulated together to form a large CAI. This suggests the possibility that during the CAI formation, O isotopic environment of CAI-forming region in the solar nebula repeatedly changed from ^{16}O-rich to ^{16}O-poor.

Introduction

Since the falling of the Allende meteorite, calcium and aluminum-rich inclusions (CAIs) found in carbonaceous meteorites have been considered as important objects to the study origin of the solar system. Larimer and Anders (1970) and Marvin et al. (1970) suggested that CAIs are probably aggregates of the highest temperature condensates from the solar nebula. Minerals in CAIs correspond to high-temperature condensates from gas of solar composition over a range of $P_{tot} = 10^{-3}$ to 10^{-6} atm (Yoneda and Grossman, 1995). CAIs are also believed to be among the oldest objects formed in the early solar system (Allégre et al., 1995).

The petrographic textures and crystal chemical properties indicate that coarse-grained CAIs appear to have experienced a molten or partially molten state in the solar nebula. However, oxygen isotope ratios are heterogeneously distributed among the constituent minerals. In a three-isotope diagram of oxygen isotope ratios, CAI minerals generally fall along a carbonaceous chondrites anhydrous mineral mixing line (CCAM) having a slope of almost unity. Spinel is enriched in ^{16}O

($\delta^{18}O = \sim-40$ ‰), whereas the ^{16}O-enrichments decrease in fassaite ($\delta^{18}O = -20$ to -40 ‰), melilite ($\delta^{18}O = \sim0$ ‰) and anorthite ($\delta^{18}O = \sim0$ ‰) (Clayton et al., 1977; Clayton 1993). Crystallization sequence from CAI melt is inconsistent with this order of ^{16}O-enrichments (Stolper, 1982). Therefore, O isotopic exchange between nebular gas and liquid during the cooling stage of CAI melt cannot explain the heterogeneous O isotopic distribution.

Diffusive exchange during post crystallization of CAIs between nebular gas and solids may be a possible explanation (Clayton and Mayeda, 1977). However, diffusion studies indicate that it is difficult to explain observed oxygen isotope distribution among CAI minerals by solid-gas diffusive exchange (Yurimoto et al., 1989; Ryerson and McKeegan, 1994). The absence of diffusion profiles among CAI minerals having different ^{16}O-enrichments argues that the gas-solid diffusive exchange is an unlikely main process for the observed inter-mineral heterogeneity of oxygen isotopes (Yurimoto et al., 1994; 1998). Yurimoto et al. (1998) suggested that O isotopic heterogeneity in CAIs be achieved by multiple flash partial melting events in the solar system. Although origin of heterogeneous O isotopic distribution in CAIs is still controversial, the heterogeneous O isotopic distribution indicates that

G. L. Kim, glkim5644@yahoo.co.jp Corresponding author
H. Yurimoto, yuri@geo.titech.ac.jp
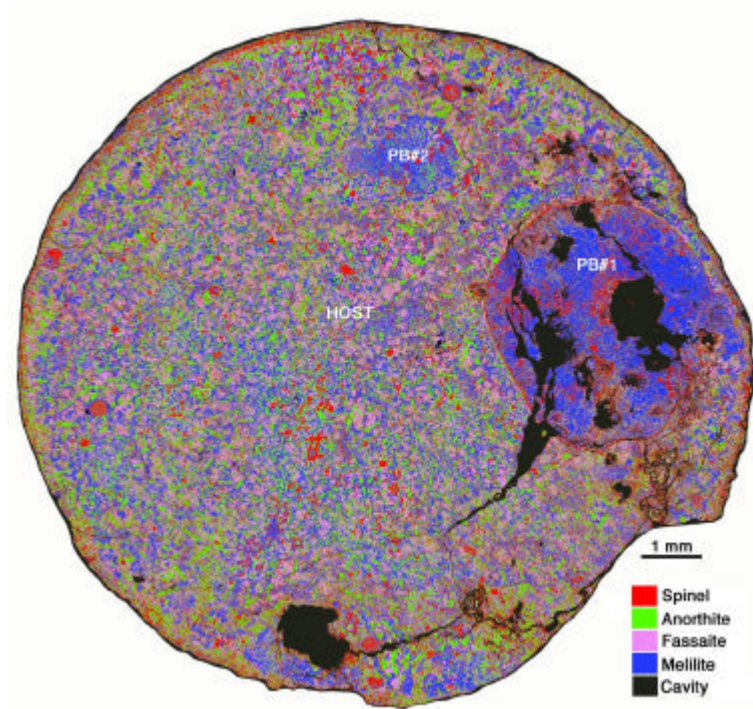
Figure 1. Mineral assemblage image of a spherical CAI from Allende chondrite, SS-02. SS-02 contains many framboids and palisade bodies. The palisade body #1 (PB#1) is completely surrounded by a spherical shell of spinel and palisade body #2 (PB#2) is surrounded by incomplete spinel chains.

disequilibrium chemical processes were essential to CAI-forming scenario.

Coarse-grained CAIs have long chain, ring and clump like arrangement of spinel crystals. Texture of spinel grains in CAIs of carbonaceous chondrites is divided into two types, i.e. "framboids" and "palisades" (Wark and Lovering, 1982a). Wark and Lovering (1982a) indicated that spinel "framboids" are produced by near-solidus processes rather than liquid crystallization and are easily produced in incomplete melts rather than completely melts from high temperature experiments. They also suggested that "palisades" did not form by familiar igneous or metamorphic processes. Therefore, they considered that "palisades" have an external origin. On the other hand, Simon and Grossman (1997) proposed that palisade bodies formed *in-situ* in the melt during CAI crystallization based on their high temperature experiments. They also interpreted "framboids" as polar or near-polar sections through palisade bodies and therefore do not make a genetic distinction between the two features. If palisades have an *in-situ* origin, O isotopic distribution in the palisades must be similar to those of the host part in CAI. If O isotopic distribution is different between palisades and the host, at least some palisades have an external origin.

Recently, McKeegan et al. (1998) reported that all CAI minerals were originally ^{16}O-rich from Semarkona CAI that is isotopically homogeneous and contains high ^{16}O-rich melilite. Krot et al. (2002) also reported that CAIs and AOAs formed in a spatially restricted region of the solar nebula containing ^{16}O-rich gas from CAI accretionary rims and amoeboid olivine aggregates (AOAs) that are ^{16}O enriched at the level inside CAIs. These indicate that the gas in the nebular region where formed CAIs was ^{16}O-rich.

Here we present *in-situ* oxygen isotopic measurements in a Type B CAI containing large palisade bodies by secondary ion mass spectrometry (SIMS). We discuss origin of the palisades and oxygen-isotopic environment in the CAI forming region using their oxygen-isotopic distribution. The preliminary results show that ^{16}O-enriched melilite grains coexisted with ^{16}O-depleted normal melilite grains in the CAI (Kim et al., 1998).

Analytical procedures

The polished section of the SS-02 from the Allende CV3 chondrite was analyzed by scanning electron microscopy (SEM: JEOL JSM-5400, University of Tsukuba).
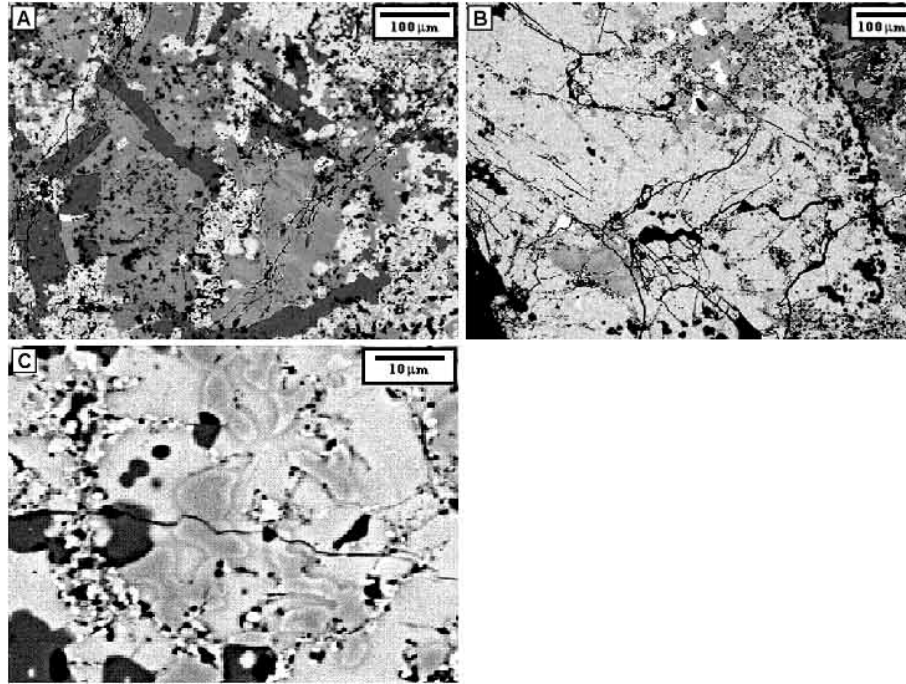
Figure 2. Detailed textures of the host, PB#1 and PB#2 in SS-02. Black corresponds to spinel, dark-gray is anorthite, gray is fassaite and bright-gray is melilite. (A) Host part. Anorthite of the host part is euhedral to subhedral lath crystal, and exist interstitially among the other phases. Fassaite is anhedral, and seems to be enclosed by melilite. (B) PB#1. Melilite is dominant in PB#1 and anorthite is not observed. White grains are perovskite. (C) PB#2. Fassaite and anorthite grains in PB#2 are small, and have irregular curved shapes.

Qualitative and quantitative chemical analyses were made by the SEM equipped with energy dispersive X-ray spectrometer (EDS: Oxford LINK-ISIS). The analytical condition was at 20 kV accele rating voltage with a beam current of 3 nA, and measurement time of 100 seconds for each point. The X-ray data were corrected by ZAF methods for quantitative analyses.

After qualitative and quantitative chemical analyses, oxygen isotopic analyses of the sample were made by SIMS. The polished sample was coated with 30 nm of gold film for SIMS analysis to eliminate the electrostatic charge on the sample surface. Oxygen isotopic measurements were performed with the TiTech Cameca ims 1270 SIMS instrument using a ~5µm diameter Cs^+ beam and an electron flood gun to compensate for electrostatic charging on sample surface. Negative secondary ions were measured at high mass resolving power (M/?M~6000) using an electron multiplier. Data were collected for dead time of detection system, and instrumental mass fractionation utilizing terrestrial standards (Yurimoto et al., 1998). Standard deviation determined by count statistics is ~3 ‰ per analysis spot and reproducibility and accuracy are ~5 ‰ in the SMOW scale.

Results

Petrography

The CAI, SS-02, from Allende meteorite is ~10 mm across and spherical in shape (Fig. 1). Many spinel framboids and palisade bodies are scattered in the CAI. Two large palisade bodies were recognized on the

Table 1. Bulk compositions of the SS-02. Bulk compositions were normalized to 100 wt % to correct for beam loss in cracks and cavities. Bulk compositions of the host and PB#1 are similar to that of Type B2 and Type B1, respectively. (* after Wark and Lovering, 1982b)

	HOST	PB#1	PB#2	*Type B1	*Type B2
Na_2O	0.18	0.00	-	0.22	0.5
MgO	10.69	7.68	6.79	10.2	11.6
Al_2O_3	28.22	29.99	31.43	29.9	26.7
SiO_2	33.17	28.10	29.37	28.6	32.9
K_2O	-	-	-	0.01	0.02
CaO	25.75	31.81	29.96	29.2	25.9
TiO_2	1.28	1.46	1.92	1.29	1.46
Cr_2O_3	0.04	0.03	0.04	0.05	0.05
FeO	0.48	0.15	0.30	0.69	0.88
NiO	0.19	0.78	0.20	0.08	0.07
Total	100.00	100.00	100.00	100.24	100.08

3
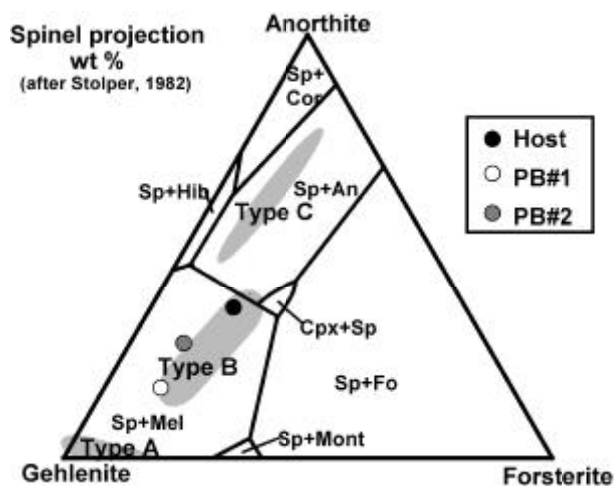
Figure 3. Bulk compositions of host, PB#1 and PB#2 projected from spinel onto the gehlenite-anorthite-forsterite plane. Bulk composition of the SS-02 (PB#1, PB#2 and host part) belongs to region of Type B CAIs.

polished surface of SS-02. We defined the surrounding areas of the palisade bodies as a host part of SS-02.

Mineral assemblage of the host part is fassaite (31 vol%), melilite (26 vol%), anorthite (28 vol%) and spinel (15 vol%). The host part is structurally unzoned so that the melilite, fassaite, spinel and anorthite are not arranged in any obvious pattern (Fig. 1). Melilite in the host part is fine-grained and anhedral (~100 µm across). Composition of the melilite ranges from $Åk_1$ to $Åk_{82}$. Anorthite in the host part is euhedral to subhedral lath-shaped crystal (~500µm in long axis, ~100 µm in short axis), and exists interstitially among the other phases (Fig. 2a). Fassaite is anhedral (~500µm), and seems to be enclosed by melilite. The fassaite typically shows sector zoning, and the boundary between fassaite and melilite is sharp. Anorthite and fassaite grains are intimately interlocking each other. Spinel crystals are present as separately and/or clumpy. Spinel crystals are euhedral to subhedral, and are poikilitically enclosed by melilite, anorthite and fassaite. Minor phases in the host part are monticellite, grossular, Fe-Ni metal and Fe-sulfide. Monticellite and grossular may be secondary alteration products of alteration of melilite. Rim of SS-02 is composed of olivine, clinopyroxene, Fe-rich spinel, Na-contained phase and alteration products of melilite. Typical Wark-Lovering rim sequences (Wark and Lovering, 1977) are not observed.

Palisade body #1 (PB#1) is ~4 mm across and completely surrounded by a spherical spinel shell (Fig. 1). Coarse melilite crystals are the most abundant (57 vol %) (Fig. 2b). Other major minerals are spinel (19 vol %) and

Table 2. Oxygen isotopic data (‰) for the SS-02 CAI from Allende meteorite. All Error are $1\sigma_{mean}$.

Area	Phase	Analysis#	$\delta^{17}O_{SMOW}$	$\delta^{18}O_{SMOW}$
Host	spinel	SpH02-1	-38.8 ± 3.3	-39.5 ± 1.9
		SpH03	-28.5 ± 2.9	-22.6 ± 2.2
		SpH04	-28.6 ± 2.7	-24.8 ± 1.9
		SpH05	-39.1 ± 3.1	-31.5 ± 1.9
		SpH06-1	-29.3 ± 2.9	-28.3 ± 2.1
		SpH07	-32.6 ± 3.2	-25.0 ± 1.8
		SpH08	-37.5 ± 2.9	-35.8 ± 2.2
		SpH09	-29.8 ± 2.9	-30.2 ± 2.2
		SpH10	-36.6 ± 3.2	-35.7 ± 1.9
	fassaite	FasH01-1	-35.2 ± 2.8	-31.5 ± 2.0
		FasH05-1	-26.2 ± 3.2	-20.5 ± 2.0
		FasH06	-28.5 ± 3.0	-24.3 ± 1.9
	mellilite	MelH01-1	-23.3 ± 3.0	-22.7 ± 1.8
		MelH02	-28.1 ± 3.1	-20.0 ± 1.8
		MelH05	-17.7 ± 3.3	-19.1 ± 1.9
		MelH07	-21.4 ± 2.9	-22.1 ± 2.0
		MelH08	-20.7 ± 3.0	-21.8 ± 2.2
		MelH09	-29.6 ± 2.7	-23.5 ± 2.3
		MelH10	-18.7 ± 2.6	-16.5 ± 1.9
	anorthite	AnH01-1	-21.6 ± 3.0	-23.5 ± 1.8
		AnH02	-28.6 ± 2.6	-18.8 ± 1.9
		AnH03	-25.6 ± 2.9	-21.0 ± 1.9
		AnH07	-22.8 ± 2.7	-15.3 ± 1.9
		AnH08	-19.6 ± 3.0	-16.3 ± 1.9
		AnH09	-27.8 ± 3.1	-23.3 ± 2.0
		AnH10	-23.0 ± 3.2	-13.5 ± 2.0
PB#1	spinel	Sp13-1	-43.3 ± 3.0	-45.5 ± 1.7
		Sp07-1	-34.2 ± 3.3	-35.9 ± 2.0
		Sp05-1	-44.3 ± 3.2	-36.3 ± 2.0
		Sp08-2	-44.5 ± 3.1	-48.9 ± 1.7
		Sp14-1	-35.8 ± 2.6	-30.5 ± 2.1
	fassaite	Fas01	-27.5 ± 2.9	-26.0 ± 1.8
		Fas02	-38.4 ± 3.1	-30.5 ± 1.9
		Fas03-1	-18.4 ± 3.0	-12.3 ± 1.8
		Fas04	-4.6 ± 3.2	-4.7 ± 2.0
		Fas05	2.3 ± 3.6	9.9 ± 1.8
		Fas06	-28.0 ± 3.1	-27.7 ± 1.9
		Fas07	-23.2 ± 3.1	-19.7 ± 2.0
		Fas08	0.4 ± 2.7	6.2 ± 2.0
		Fas09	-21.7 ± 2.9	-20.9 ± 1.9
		Fas10	-21.4 ± 2.7	-17.1 ± 2.2
		Fas11	-31.0 ± 2.7	-28.3 ± 2.1
		Fas12	-32.3 ± 2.8	-34.2 ± 1.8
		Fas13	-16.3 ± 2.8	-10.8 ± 2.0
	melilite	Mel03	-6.4 ± 2.8	-2.9 ± 1.9
		Mel04	-2.3 ± 3.0	-2.7 ± 1.8
		Mel06	0.5 ± 3.1	2.8 ± 2.0
		Mel07	4.0 ± 2.6	7.2 ± 1.8
		Mel08	2.5 ± 2.8	7.5 ± 2.2
		Mel11	-1.4 ± 3.0	-1.8 ± 2.2
		Mel12	-1.7 ± 2.8	3.9 ± 1.7
		Mel13	-7.3 ± 2.7	-2.8 ± 2.0
		Mel14	-7.5 ± 2.9	-2.9 ± 2.2
	perovskite	Pv02-1	-2.2 ± 3.0	-2.2 ± 2.4
		Pv03	-4.2 ± 3.4	-4.4 ± 2.1
PB#2	spinel	Sp01	-36.0 ± 3.1	-32.2 ± 2.3
	melilite	Mel01	-14.1 ± 3.2	-6.9 ± 2.0
	fassaite	Fas01	-27.8 ± 2.7	-31.1 ± 1.9
	anorthite	An01	-4.7 ± 2.9	-4.6 ± 1.9
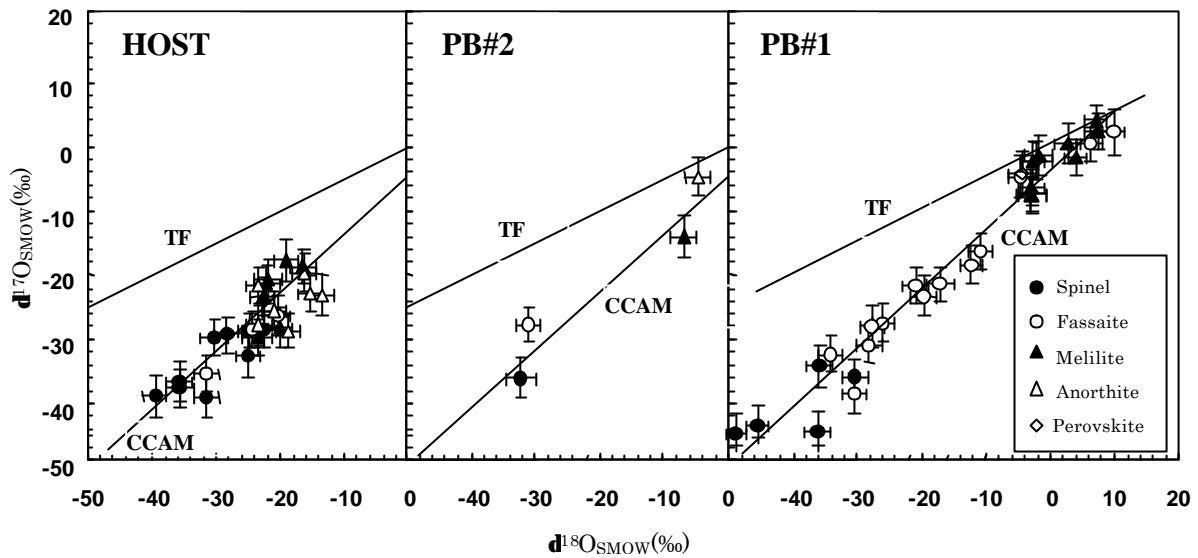
Figure 4. Oxygen isotopic compositions of each part in SS-02. All data plots along the CCAM line. All minerals in host show ^{16}O enrichment. However, in PB#1, melilite, anorthite and some fassaite grains plot near the terrestrial fractionation (TF) line. In PB#2, oxygen isotopic composition of melilite shows intermediate ^{16}O excesses between those in the host and in PB#1 melilite.

fassaite (14 vol %). Melilite composition in the PB#1 is gehlenite-rich and ranges from $Åk_6$ to $Åk_{48}$. Spinel in the PB#1 is euhedral to subhedral, and the size is ~30μm or less. The spinel is poikilitically enclosed by melilite and fassaite. Spinel crystals tend to concentrate near the center of PB#1. Spinel framboids are also present in the PB#1. Perovskite (~50μm) is enclosed by fassaite and among spinel grains in the center of PB#1. Fassaite crystals with irregular shape (~100μm) are present. Sector zonings are observed in the fassaite crystals. Anorthite was not observed in the PB#1. Alteration phases in PB#1 are similar to in the host. Grossular often exists near PB#1 spinel chain.

The second large palisade body (PB#2) in Figure 1 is mainly composed of melilite, fassaite, spinel and anorthite, and surrounded by incomplete spinel chains. Melilite is the most dominant mineral in the PB#2 and the composition ranges from Åk9 to Åk46, which is similar to those of PB#1. Fassaite grains are very small (~ 15μm), and have irregular and rounded shape (Fig. 2c). Anorthite crystal is also small and irregular.

The results of bulk composition of the host and PB#1 are shown in Table 1. The bulk composition of PB#1, PB#2 and the host part are plotted in the region of type-B CAIs (Fig. 3). The bulk composition of PB#1 is most refractory which is consistent with the melilite composition in it. The PB#2 is intermediate and the host part is least refractory.

Oxygen isotopic compositions of SS-02

The oxygen isotopic ratios are given in Table 2. The data points for all refractory phases in the host show ^{16}O excesses relative to SMOW and fall on the CCAM line (average value: melilite: (δ^{17}O, δ^{18}O) = (-23 ‰, -21 ‰), anorthite: (-24‰, -19‰), spinel: (-33 ‰, -30 ‰), fassaite: (-30 ‰, -25‰)) (Fig. 4).

In the PB#1, spinel shows ^{16}O excesses (-40 ‰, -39 ‰) and falls on the CCAM line, fassaite has variations of oxygen isotopic composition along the CCAM line (δ^{17}O = -38 ~ +3 ‰; δ^{18}O = -34 ~ +10 ‰). In contrast, melilites and perovskites in the PB#1 have oxygen isotopic compositions close to the intersection of the CCAM line and the terrestrial fractionation line (average value: (-2 ‰, +1 ‰) and (-3 ‰, -3 ‰), respectively).

Spinel and fassaite in the PB#2 show ^{16}O excesses ((-36 ‰, -32 ‰) and (-28 ‰, -31 ‰), respectively). Anorthite in the PB#2 shows ^{16}O-poor composition (-5 ‰, -5 ‰). Melilite in the PB#2 shows ^{16}O excesses but less than those in the host (δ^{17}O = -14 ‰; δ^{18}O = -7‰).

Dicussion

The spherical shapes and igneous textures of PB#1, PB#2 and the host part suggest that each part appears to have experienced a molten or partially molten state. If

the SS-02 CAI was crystallized from a single liquid droplet, oxygen isotopic distribution must be similar among the PB#1, PB#2 and the host part, i.e., oxygen isotopic compositions of each CAI mineral in the palisades and in the host must have similar distributions. However, all refractory minerals in the host show ^{16}O-enrichment. Whereas in the palisades, spinel shows ^{16}O-enrichment and melilite and anorthite shows ^{16}O-depletion. Moreover, fassaite in the palisade cover the total range of O isotopic heterogeneity in the palisade minerals from ^{16}O-rich to ^{16}O-poor. These O isotopic distributions cannot be explained by O isotopic exchange between nebular gas and liquid during cooling stage of CAI melt.

These O isotopic distributions are also difficult to produce by solid-state O isotopic exchange after solidification of the SS-02 for the following reasons: (1) O isotopic heterogeneities among minerals or O isotopic disturbances are larger in the palisades than in the surrounding host. (2) Grain sizes of minerals are larger in the palisades than in the host. If solid-state isotopic exchanges occurred in the SS-02, O isotopic compositions in the host mineral grains are more easily disturbed than those in the palisade minerals. Therefore, these results indicate that each component analyzed in this study were formed separately and gathered together into the SS-02 in the late stage.

From the igneous texture of SS-02, crystallization sequence of the host part is spinel, melilite, anorthite and fassaite, in order of decreasing temperature. Crystallization sequence from phase diagram (Fig. 3) is consistent with the crystallization sequence. All refractory phases in the host show ^{16}O-rich in the order of spinel > fassaite ~ melilite ~ anorthite (Fig. 4). The enrichment order is not inconsistent with the above crystallization sequence. Therefore, the host part simply crystallized from ^{16}O-rich liquid with some O isotopic exchanges between the liquid and solar nebula gas during crystallization.

In PB#1, melilite composition near the palisade spinel rim is gehlenitic but becomes less gehlenitic in center. This result shows that melilite in PB#1 is crystallized from the rim first and grew the inward. From the bulk composition, the inferred crystallization sequence of PB#1 is spinel, melilite and fassaite in order of decreasing temperature. The crystallization sequences are consistent with those inferred from the texture. On the other hand, spinel and some fassaite grains in PB#1 and PB#2 are enriched in ^{16}O (Fig. 4). But melilite and anorthite are depleted in ^{16}O. O isotopic distribution of the fassaite varied from ^{16}O-rich endmember to ^{16}O-poor endmember in the palisade. Oxygen isotopic distribution

among minerals in PB#1 and PB#2 are similar to those of previous studies (Clayton et al., 1977; Clayton 1993). These observations are essentially the same as the CAI reported by Yurimoto et al. (1998). According to Greenwood et al. (1996), melting speed above liquidus is in the order of melilite, anorthite and fassaite. Therefore, the multiple flash partial melting processes in the solar nebula proposed by Yurimoto et al. (1998) can be applied to interpret the heterogeneous O isotope distribution among the minerals in PB#1 and PB#2. The small fassaite grains having eroded shapes in PB#2 that are trapped in melilite support the multiple melting processes as textural evidence (Fig. 2c). Thus, the variation of oxygen isotopes in the palisade bodies was generated before the trapping of the palisades into the host of SS-02, i.e., O isotopic environment formed the palisade bodies was ^{16}O-poor. In contrast, the environment formed the host was ^{16}O-rich.

The distinct feature of heterogeneous oxygen distribution among PB#1, PB#2 and the host part clearly indicates that SS-02 is an aggregate, i.e., a compound CAI. The O isotopic distribution in the palisades and the host of SS-02 indicates that the palisades formed before the host formation. Therefore, degree of O isotopic exchange in CAI-forming region changes with time and space. Such O isotopic fluctuation support that CAIs formed near inner edge of gas disk of the solar nebula. O isotopic environment near the inner edge repeatedly changes from ^{16}O-rich to ^{16}O-poor (Yurimoto et al., 2001).

Conclusions

A compound CAI, SS-02, containing big palisade bodies (PB#1 and PB#2) was found within the Allende meteorite. All refractory phases in the host show ^{16}O-rich compositions. Oxygen isotopic distribution among minerals in PB#1 and PB#2 are similar to those of previous studies (Clayton et al., 1977; Clayton 1993). Oxygen isotopic compositions, textures, and bulk compositions of PB#1 and PB#2 in SS-02 are very different from their host. The results indicate that the palisades formed before the host part and oxygen isotope exchange of the palisade bodies occurred before the trapping of palisades into the host. These are evidence that the palisade bodies in SS-02 were formed not *in-situ* but have an external origin. Therefore, SS-02 is an aggregate of CAIs, i.e., a compound CAI. The O isotopic distribution in SS-02 suggests the possibility that O isotopic environments of CAI-forming region repeatedly change from ^{16}O-rich to ^{16}O-poor. Such the change of O-isotopic environments may be common in the CAI

forming region.

Acknowledgements

References

Allègre C. J., Manhès G., and Gòpel C. (1995) The age of Earth. Geochimica et Cosmochimica Acta 59, 1445-1456.

Clayton R. N. and Mayeda T. K. (1977) Correlated oxygen and magnesium isotopic anomalies in Allende inclusions. I: Oxygen. Geophysical Research Letters A, 295-298.

Clayton R. N., Onuma N., Grossman L., and Mayeda T. K. (1977) Distribution of pre-solar component in Allende and other carbonaceous chondrites. Earth and Planetary Science Letter 34, 209-224.

Clayton R. N. (1993) Oxygen isotopes in meteorites. Annual Review of Earth and Planetary Sciences 21. 115-149.

Greenwood J. P. and Hess P. C. (1996) Congruent melting kinetics: constraints on chondrule formation. In Chondrules and the Protoplanetary Disk (R. H. Hewins, et al., Eds.). Cambridge Univ. Press, Cambridge, UK, 205-211.

Kim, G.L., Yurimoto, H. and Sueno, S. (1998) ^{16}O-enriched melilite and anorthite coexisting with ^{16}O-depleted melilite in a CAI. In Lunar and Planetary Science XXIX, Abstract #1344, Lunar and Planetary Institute, Houston (CD-ROM).

Kort A. N., McKeegan K. D., Leshin L. A., MacPherson G. J. and Scott E. R.D (2002) Existence of an ^{16}O-rich gaseous reservoir in the solar nebula. Science 295, 1051-1054.

Larimer J. W. and Anders E. (1970) Chemical fractionations in meteorites-III. Major element fractionations in chondrites. Geochimica et Cosmochimica Acta 34, 367-387.

Marvin U. B., Wood J. A., and Dickey J. S., Jr. (1970) Ca-Al-rich phases in Allende meteorite. Earth and Planetary Science Letter 7, 346-350.

Mckeegan K. D., Leshin L. A., Russell S. S. and MacPherson G. J.

(1998) Oxygen isotopic abundances in calcium-aluminum-rich inclusions from ordinary chondrites: implications for nebular heterogeneity. Science 280, 414-418.

Ryerson F. J. and Mckeegan K. D. (1994) Determination of oxygen self-diffusion in åkermanite, anorthite, diopside and spinel: implications for oxygen isotopic anomalies and thermal histories of Ca-Al-rich inclusion. Geochimica et Cosmochimica Acta 58, 3713-3734.

Simon S. B. and Grossman L. (1997) In situ formation of palisade bodies in calcium, aluminum-rich refractory inclusions. Meteoritics & Planetary Science 32, 61-70.

Stolper E. (1982) Crystallization sequences of Ca-Al-rich inclusions from Allende: An experimental study. Geochimica et Cosmochimica Acta 46, 2159-2180.

Wark D. A. and Lovering J. F. (1977) Maker events in the early evolution of the solar system: Evidence from rims on Ca-Al-rich inclusion in carbonaceous chondrites. Proceeding of 8th Lunar Science Conference, 95-112.

Wark D. A. and Lovering J. F. (1982a) Evolution of Ca-Al-rich bodies in the earliest solar system: Growth by incorporation. Geochimica et Cosmochimica Acta 46, 2595-2607.

Wark D. A. and Lovering J. F. (1982b) The nature and origin of Type B1 and Type B2 Ca-Al-rich inclusions in the Allende meteorite. Geochimica et Cosmochimica Acta 46, 2581-2594.

Yoneda S. and Grossman L. (1995) Condensation of CaO-MgO-Al$_2$O$_3$-SiO$_2$ liquids from cosmic gases. Geochimica et Cosmochimica Acta 59, 3413-3444.

Yurimoto H., Nagasawa H., Mori Y., and Matsubaya O. (1994) Micro-distribution of oxygen isotopes in a refractory inclusion from the Allende meteorite Earth and Planetary Science Letter 128, 47-53.

Yurimoto, H., Ito, M. and Nagasawa, H. (1998) Oxygen isotope exchange between refractory inclusion in Allende and solar nebula gas. Science 282, 1874-1877.

Yurimoto H, Y Asada, and K Hirai (2001) Oxygen isotopic composition of fine-grained CAIs and genetic relation to coarse-grained CAIs. Meteoritics & Planetary Science 36, No. 9, A230.